

BULLETIN DE L'ASSOCIATION MINERALOGIQUE DU CANADA

# THE CANADIAN MINERALOGIST

JOURNAL OF THE MINERALOGICAL ASSOCIATION OF CANADA

Volume 32

March 1994

Part 1

*The Canadian Mineralogist*  
Vol. 32, pp. 1-14 (1994)

## DETERMINATION OF THE MEGASTRUCTURES OF THE BORATE POLYMORPHS PRINGLEITE AND RUITENBERGITE

JOEL D. GRICE

*Mineral Sciences Section, Canadian Museum of Nature, P.O. Box 3443, Station D, Ottawa, Ontario K1P 6P4*

PETER C. BURNS AND FRANK C. HAWTHORNE

*Department of Geological Sciences, University of Manitoba, Winnipeg, Manitoba R3T 2N2*

### ABSTRACT

The new species pringleite and ruitenbergite from the Potash Company of America mine near Sussex, New Brunswick, are dimorphous; a crystal-structure analysis has established their formula as  $\text{Ca}_9\text{B}_{26}\text{O}_{34}(\text{OH})_{24}\text{Cl}_4 \cdot 13\text{H}_2\text{O}$ . Pringleite is triclinic  $P\bar{1}$ , with  $a$  12.746(2),  $b$  13.019(3),  $c$  9.693(2) Å,  $\alpha$  102.2(2),  $\beta$  102.1(2),  $\gamma$  85.6(1)°,  $Z$  = 1. Ruitenbergite is monoclinic  $P2_1$ , with  $a$  19.857(7),  $b$  9.708(4),  $c$  17.522(6) Å,  $\beta$  114.68(3)°,  $Z$  = 2. The  $R$  index for pringleite is 4.5% for 4918 observed reflections, and for ruitenbergite, it is 9.3% for 1704 observed reflections. These megastructures each have 110 atoms per asymmetric unit, excluding H positions. The closely related structures have a zeolite-like borate framework with large channels containing the interstitial Ca species,  $\text{H}_2\text{O}$  groups and hydrogen-bonded Cl atoms. The framework has 12 B atoms in triangular and 14 in tetrahedral coordination in each case. There is a distinctive 12-membered borate ring forming planes that are cross-linked by further polymerization of the borate groups. The configuration of the B polyhedra in the rings and cross-linkage serves to distinguish the two polymorphs.

**Keywords:** pringleite, ruitenbergite, polymorphism, crystal structure, borate, megastructure.

### SOMMAIRE

La pringleite et la ruitenbergite, nouvelles espèces minérales découvertes à la mine dite Potash Company of America, près de Sussex, au Nouveau Brunswick, sont dimorphiques. Une ébauche de leur structure cristalline a établi leur formule chimique:  $\text{Ca}_9\text{B}_{26}\text{O}_{34}(\text{OH})_{24}\text{Cl}_4 \cdot 13\text{H}_2\text{O}$ . La pringleite est triclinique  $P\bar{1}$ , avec  $a$  12.746(2),  $b$  13.019(3),  $c$  9.693(2) Å,  $\alpha$  102.2(2),  $\beta$  102.1(2),  $\gamma$  85.6(1)°,  $Z$  = 1. La ruitenbergite est monoclinique  $P2_1$ , avec  $a$  19.857(7),  $b$  9.708(4),  $c$  17.522(6) Å,  $\beta$  114.68(3)°,  $Z$  = 2. Nous avons affiné la structure de la pringleite jusqu'à un résidu  $R$  de 4.5% (4918 réflexions observées), et celle de la ruitenbergite, jusqu'à un résidu  $R$  de 9.3% (1704 réflexions observées). Ces mégastructures possèdent plus de 110 atomes par unité asymétrique, sans compter les atomes d'hydrogène. Ces structures sont très semblables, et sont faites d'une trame de groupes de borate ressemblant à une zéolite; les canaux contiennent les espèces interstitielles à Ca, les groupes de  $\text{H}_2\text{O}$  et les atomes de Cl, qui participent à des liaisons hydrogène. La trame contient 12 atome de B à coordinence [3] et quatorze à coordinence [4] dans chaque cas. Chaque structure contient un anneau distinctif à douze groupes de borate, qui constitue un plan structural; ces plans sont liés par d'autres groupes polyédriques de borate. C'est la configuration des polyèdres de B dans les anneaux et dans les agencements entre ceux-ci qui distinguent les polymorphes.

(Traduit par la Rédaction)

**Mots-clés:** pringleite, ruitenbergite, polymorphisme, structure cristalline, borate, mégastructure.

## INTRODUCTION

Pringleite and ruitenbergite, polymorphs with the idealized formula  $\text{Ca}_9\text{B}_{26}\text{O}_{34}(\text{OH})_{24}\text{Cl}_4 \cdot 13\text{H}_2\text{O}$ , are two new mineral species found in the Potash Company of America mine, near Sussex, New Brunswick (Roberts *et al.* 1993). Both minerals occur in this evaporite deposit as rare anhedral grains, a few millimeters in size, usually associated with halite and hilgardite-1A, and minor sylvite, anhydrite, quartz and clays. Other borates found in this evaporite sequence are boracite, colemanite, hilgardite-4M, hydroboracite, pricelite, szaibelyite, veatchite, volkovskite (Rachlin *et al.* 1986, Roulston & Waugh 1981), trembachite (Burns *et al.* 1992) and hilgardite-1A (Roberts *et al.* 1993).

Although we were presented with results of excellent electron-microprobe analyses (Roberts *et al.* 1993), the limitations of this technique for light-element determination require a crystal-structure analysis to establish the chemical formulae necessary for the description of these new species. The success of this method as a technique to determine chemical composition was described in detail by Hawthorne & Grice (1990).

The determination of the crystal structures of pringleite and ruitenbergite marks a new era for mineral structures. Each structure has over 100 atoms (excluding H) per asymmetric unit, making them the largest (mega-)structures known to date in mineralogy.

## CRYSTAL-STRUCTURE ANALYSIS

Intensity data for determination of the crystal structure of pringleite (catalogue number 82047, Canadian Museum of Nature) and ruitenbergite (catalogue number 66920, Geological Survey of Canada) were

collected on an  $R3m$  automated four-circle diffractometer using the method of Grice & Ercit (1986). The diffractometer was operated at 50 kV and 30 mA, with graphite-monochromated  $\text{MoK}\alpha$  radiation. A unique set of intensity data up to  $2\theta = 55^\circ$  was collected using a 0:20 scanning mode. Further details of data collection are given in Table 1. The better refinement of pringleite ( $R = 4.4\%$  versus  $R = 9.4\%$  for ruitenbergite) is due to the differing quality of the crystals. Because of the very small size of the ruitenbergite crystal, the counting statistics of the intensity data set were poor; however, this material is the best available at present.

Reduction of the intensity data, determination and refinement of the structure were done using the SHELXTL PC package of programs (Sheldrick 1990). For the absorption correction, twelve intense diffraction-maxima were chosen for  $\psi$ -diffraction-vector scans, and the azimuthal  $R$  index, based on a comparison of the 35 intensity measurements for each diffraction-maximum, was minimized by modeling the crystal as an ellipsoid of known orientation. The

TABLE 2. PRINGLEITE: ATOMIC COORDINATES ( $\times 10^4$ ) AND ISOTROPIC DISPLACEMENT FACTORS ( $\text{\AA}^2 \times 10^3$ )

	<i>x</i>	<i>y</i>	<i>z</i>	<i>U</i> (eq)
Ca1	0	0	0	10(1)
Ca2	6993(2)	3050(2)	8019(2)	11(1)
Ca3	7648(2)	8770(2)	3976(2)	11(1)
Ca4	1967(2)	8075(1)	7980(2)	10(1)
Ca5	5658(2)	705(1)	1942(2)	9(1)
Ca6	641(2)	5644(2)	1807(2)	11(1)
Ca7	2679(2)	3822(2)	3988(2)	12(1)
Ca8	5001(2)	4987(1)	9941(2)	11(1)
Ca9	5350(2)	8586(2)	7293(2)	18(1)
B1	48(8)	7343(8)	4952(11)	10(2)
B2	9152(8)	8006(8)	1347(11)	9(2)
B3	2860(8)	339(8)	667(11)	9(2)
B4	5141(8)	7989(8)	1497(11)	7(2)
B5	7864(8)	5297(8)	606(11)	8(2)
B6	3571(8)	5832(8)	6933(11)	10(2)
B7	2613(8)	6437(7)	342(10)	8(2)
B8	8506(8)	764(8)	6984(11)	11(2)
B9	5026(9)	2331(8)	4974(12)	14(2)
B10	7683(8)	1483(8)	546(11)	9(2)
B11	154(9)	2947(9)	1535(12)	15(2)
B12	4141(8)	2996(8)	1322(11)	11(2)
B13	4174(9)	9043(8)	9719(11)	11(2)
B14	9042(8)	2068(8)	9322(11)	11(2)
B15	802(7)	7379(7)	132(10)	6(2)
B16	3634(9)	1774(8)	2743(11)	11(2)
B17	8665(9)	6733(8)	2718(11)	12(2)
B18	6805(9)	1324(8)	5243(12)	14(2)
B19	8234(9)	9799(8)	1643(11)	11(2)
B20	3177(8)	4768(8)	1459(11)	11(2)
B21	9207(8)	3997(8)	9744(11)	9(2)
B22	4043(8)	7087(8)	9286(11)	9(2)
B23	5859(9)	2403(9)	278(12)	17(2)
B24	4526(9)	4052(8)	6680(12)	14(2)
B25	1905(8)	6433(8)	5156(11)	10(2)
B26	9403(8)	8947(7)	6733(10)	7(2)
	01	9724(5)	6688(5)	3661(7)
	02	9372(5)	8130(5)	5430(7)
	03	1082(5)	7206(5)	5661(7)
	04	9923(5)	7301(5)	886(7)
	05	8964(5)	8968(5)	993(7)
	06	8519(5)	7717(5)	2174(7)
	07	3668(5)	842(5)	1601(7)
	08	4959(5)	2323(5)	971(7)
	09	3066(5)	9416(5)	9764(7)
	010	4887(5)	7066(5)	574(7)
	011	3512(5)	2744(5)	2190(7)

TABLE 1. DATA COLLECTION DETAILS FOR THE CRYSTAL STRUCTURES OF PRINGLEITE AND RUITENBERGITE

Ideal Formula: $\text{Ca}_9\text{B}_{26}\text{O}_{34}(\text{OH})_{24}\text{Cl}_4 \cdot 13\text{H}_2\text{O}$	
Space Group	<i>P</i> 1
<i>a</i> ( $\text{\AA}$ )	12.746(2)
<i>b</i>	13.019(3)
<i>c</i>	9.693(2)
$\alpha(^{\circ})$	102.2(2)
$\beta$	102.1(2)
$\gamma$	85.6(1)
<i>V</i> ( $\text{\AA}^3$ )	1536.2(5)
Unique reflections	7507
Observed reflections	4918 [ $5\sigma(F)$ ]
Crystal size (mm)	0.25x0.25x0.20
Min. transmission	0.833
Max. transmission	0.859
<i>R</i> (observed) %	4.5
<i>wR</i> (observed) %	3.9

TABLE 2 — (Part 2)

012	4809(5)	8948(5)	1174(7)	10(1)
013	8061(5)	4405(5)	9710(7)	11(1)
014	8683(5)	5824(5)	1562(7)	11(1)
015	4121(5)	8049(5)	8712(6)	8(1)
016	2749(5)	6496(5)	6442(7)	13(1)
017	3803(5)	4882(5)	6107(7)	10(1)
018	4229(5)	6133(5)	8244(7)	9(1)
019	2984(5)	7109(5)	9629(7)	10(1)
020	3262(5)	5593(5)	662(7)	13(1)
021	1623(5)	6618(5)	656(7)	10(1)
022	9179(5)	1077(5)	8315(7)	11(1)
023	8677(5)	9791(5)	6182(7)	11(1)
024	7666(5)	1402(5)	6551(7)	13(1)
025	5994(5)	2087(5)	5797(7)	10(1)
026	4685(5)	1679(5)	3691(7)	11(1)
027	4411(5)	3190(5)	5408(7)	14(1)
028	8322(5)	659(5)	893(7)	11(1)
029	7986(5)	2107(5)	9744(7)	12(1)
030	6679(5)	1683(5)	902(7)	13(1)
031	9918(5)	2011(5)	608(7)	10(1)
032	9130(5)	2966(5)	8741(7)	9(1)
033	9728(5)	3884(5)	1240(7)	14(1)
034	3931(5)	3931(5)	909(7)	10(1)
OH1	1789(6)	684(6)	502(8)	23(2)
OH2	5811(5)	7988(5)	2826(7)	18(1)
OH3	4738(5)	9804(5)	9255(7)	15(1)
OH4	6818(5)	5692(5)	550(8)	19(1)
OH5	884(6)	2956(5)	2800(8)	19(2)
OH6	487(5)	7129(5)	8545(7)	15(1)
OH7	1175(5)	8455(5)	338(7)	12(1)
OH8	2751(5)	1812(5)	3496(7)	13(1)
OH9	7747(5)	6794(5)	3414(7)	16(1)
OH10	7143(5)	1635(5)	4023(7)	16(1)
OH11	6439(5)	258(5)	4606(7)	15(1)
OH12	7128(5)	9458(5)	1463(7)	12(1)
OH13	8641(5)	82(5)	3189(7)	16(1)
OH14	3584(5)	5126(5)	3018(8)	19(2)
OH15	2079(5)	4428(5)	1318(7)	18(1)
OH16	9837(5)	4758(5)	9405(7)	14(1)
OH17	5631(5)	2010(5)	8721(7)	16(1)
OH18	6200(5)	3492(5)	507(7)	16(1)
OH19	4171(5)	3774(5)	7902(7)	15(1)
OH20	5613(5)	4350(5)	7344(7)	13(1)
OH21	1492(5)	5356(5)	4515(7)	14(1)
OH22	2247(7)	6680(6)	3911(9)	30(2)
OH23	8919(5)	8640(5)	7823(7)	15(1)
OH24	481(5)	9317(5)	7473(7)	16(1)
C11	2625(3)	8958(3)	3347(3)	36(1)
C12	6698(3)	5720(2)	5622(3)	33(1)
C13	9830(3)	4870(3)	6205(3)	38(1)
C14	3180(3)	1373(2)	7214(4)	45(1)

resulting model was used to correct the normal intensity data. Scattering curves for neutral atoms, together with anomalous dispersion corrections, were taken from Cromer & Mann (1968) and Cromer & Liberman (1970), respectively.

### Pringleite

Analysis of the intensity data indicated the noncentrosymmetric space-group  $P1$  [mean  $|E^2 - 1| = 0.723$ ]. The phasing of a set of normalized structure-factors gave an  $E$ -map with the coordinates of six heavy atoms (chosen as Ca) and 24 lighter atoms (chosen as oxygen). With three cycles of least-squares refinement, the residual index  $R$  was found to be 34%. From this initial model, a series of refinements, followed by the calculation of difference-Fourier maps, showed additional atomic sites. Refinement of all variables for an isotropic displacement model converged to an  $R$

TABLE 2 — (Part 3)

W1	6974(5)	8161(5)	6108(7)	20(2)
W2	1951(7)	3378(7)	5948(9)	34(3)
W3	640(6)	569(6)	2731(9)	30(3)
W4	12580(9)	9088(7)	6525(9)	47(4)
W5	7743(6)	3614(6)	6187(8)	27(3)
W6	6508(6)	7708(6)	9021(8)	26(3)
W7	4626(6)	7240(6)	5410(9)	34(3)
W8	6507(6)	49(6)	7977(8)	31(3)
W9	4667(6)	9714(6)	5591(9)	30(3)
W10	5476(6)	5654(6)	2570(8)	24(2)
W11	8207(6)	6516(6)	8498(9)	32(3)
W12	7978(8)	4026(9)	2941(10)	54(4)
W13	1485(8)	2867(8)	8894(13)	63(5)
H1	1756(89)	10984(87)	9947(125)	30
H2	-4104(89)	7422(87)	13025(127)	30
H7	1238(91)	8616(89)	11142(128)	30
H9	-2226(89)	6534(86)	14010(126)	30
H10	2526(90)	12086(87)	4257(127)	30
H11	-3991(89)	9996(88)	15130(125)	30
H12	6946(91)	9133(88)	10691(129)	30
H13	-1561(90)	10720(86)	13616(129)	30
H14	3413(88)	15801(86)	13502(126)	30
H15	1852(89)	3944(87)	10531(128)	30
H16	-159(89)	4716(86)	8509(127)	30
H17	-4986(89)	12285(88)	8229(128)	30
H19	3608(89)	13638(86)	7703(126)	30
H20	-4198(88)	14831(87)	6951(127)	30
H21	1261(89)	15147(88)	15121(126)	30
H22	2721(90)	6970(87)	4234(126)	30
H24	740(89)	9660(88)	7111(127)	30
HW1	6928(89)	7351(88)	5906(126)	30
HW1*	-2591(89)	8167(87)	16590(125)	30
HW2	1576(89)	13375(87)	16514(126)	30
HW3	255(95)	10590(93)	12779(134)	30
HW5	-1699(92)	13874(87)	6123(128)	30
HW5*	-2461(93)	14080(86)	5482(128)	30
HW7	4957(88)	6571(85)	5355(123)	30
HW9	4330(90)	9688(88)	5004(126)	30
HW10	5923(90)	15645(87)	13039(127)	30
HW13	-277(93)	10459(92)	13289(133)	30
HW13*	938(89)	2854(86)	8609(127)	30

\* denotes the second H atom of an  $\text{H}_2\text{O}$  group

index of 6.0%. Conversion to anisotropic displacement factors for all Ca and Cl atoms led to convergence to  $R = 4.8\%$  and  $wR = 5.2\%$ . At this point in the refinement, H atoms could be added with confidence, but not all of the H atoms present could be located. This refinement converged to  $R = 4.5\%$  and  $wR = 4.7\%$ . Table 2 contains the final positional parameters and equivalent isotropic displacement factors. There was no improvement in the refinement by assuming the enantiomorphous structure. Selected interatomic distances are presented in Table 3; observed and calculated structure-factor coefficients are available from the Depository of Unpublished Data, CISTI, National Research Council of Canada, Ottawa, Ontario, Canada K1A 0S2.

### Ruitenbergite

Ruitenbergite was solved in the same manner as pringleite. Analysis of the  $E$ -values gave a mean  $|E^2 - 1|$  equal to 0.809, indicative of the noncentrosymmetric space-group  $P2_1$ , thus excluding the other choice of space group,  $P2_1/m$ , for this diffraction symmetry and set of extinction conditions. Two factors

TABLE 3. PRINGLEITE: BOND LENGTHS (Å)

Ca1-OH1	2.433 (1)	Ca6-O21	2.422 (2)
Ca1-W3	2.561 (8)	Ca6-OH15	2.392 (2)
Ca1-O5A	2.417 (1)	Ca6-OH21	2.718 (2)
Ca1-O22A	2.399 (1)	Ca6-OH2	2.790 (2)
Ca1-O28A	2.498 (1)	Ca6-O1A	2.460 (2)
Ca1-O31A	2.559 (1)	Ca6-O4A	2.539 (2)
Ca1-OH7A	2.449 (1)	Ca6-O14A	2.448 (2)
Ca1-OH2D	2.651 (1)	Ca6-O33A	2.552 (2)
Ca1-OH2E	2.616 (1)	Ca6-OH1K	2.418 (2)
Ca2-O13	2.430 (2)	Ca7-O11	2.374 (2)
Ca2-O24	2.505 (2)	Ca7-O17	2.454 (2)
Ca2-O25	2.407 (2)	Ca7-O27	2.525 (2)
Ca2-O29	2.381 (2)	Ca7-OH5	2.559 (2)
Ca2-O32	2.673 (2)	Ca7-OH8	2.564 (2)
Ca2-OH17	2.563 (2)	Ca7-OH14	2.550 (2)
Ca2-OH20	2.432 (2)	Ca7-OH15	2.790 (2)
Ca2-W5	2.444 (10)	Ca7-OH21	2.442 (2)
Ca2-OH10	2.742 (2)	Ca7-W2	2.469 (10)
Ca3-O2	2.532 (2)	Ca8-O18	2.455 (2)
Ca3-O6	2.392 (2)	Ca8-OH19	2.367 (2)
Ca3-O23	2.449 (2)	Ca8-OH20	2.738 (2)
Ca3-OH2	2.565 (2)	Ca8-O10A	2.642 (2)
Ca3-OH9	2.523 (2)	Ca8-O20A	2.484 (2)
Ca3-OH12	2.713 (2)	Ca8-O34A	2.447 (2)
Ca3-W1	2.679 (9)	Ca8-OH4A	2.456 (2)
Ca3-OH1C	2.435 (2)	Ca8-OH10	2.465 (2)
Ca3-OH1G	2.538 (2)	Ca8-W10A	2.476 (7)
Ca4-O3	2.384 (2)	Ca9-O15	2.512 (3)
Ca4-O9	2.470 (2)	Ca9-OH3	2.430 (2)
Ca4-O15	2.688 (2)	Ca9-W1	2.541 (8)
Ca4-O16	2.546 (2)	Ca9-W6	2.412 (8)
Ca4-O19	2.352 (2)	Ca9-W7	2.333 (8)
Ca4-OH6	2.541 (2)	Ca9-W9	2.425 (9)
Ca4-OH24	2.429 (2)	Ca9-W8A	2.394 (8)
Ca4-OH7B	2.624 (2)		
Ca4-W4A	2.399 (11)		

impeded the structure solution and refinement: (1) weak intensity-data due to the small size of the crystal; (2) high correlations of atom parameters related by the pseudotranslation symmetry along the Z axis. There are very few weak reflections that define the doubling of the cell along the Z direction, and the structure was first derived for the subcell (*i.e.*, for the stronger reflections with  $l = 2n$ ). For the subcell, 4261 unique reflections were measured, of which 1532 were observed [ $F_0 > \sigma(F)$ ]. The structure solution derived by direct methods gave the coordinates of the five heavy atoms (Ca) and 12 lighter atoms. With a series of least-squares refinements, the structure refined to an *R* index of 7.0% with anisotropic displacement factors for the Ca and Cl atoms. For the true cell (*i.e.*, *c*-period doubled), 8502 unique reflections were measured, of which 1704 were observed [ $F_0 > 5\sigma(F)$ ]. Using the subcell structure as a beginning model for the true cell, the crystal structure of ruitenbergite was derived, but because of the limitations on the intensity data, the

TABLE 3 — (Cont'd.)

B(1)-O(3)	1.366 (10)	B(15)-O(21)	1.477 (10)
B(1)-O(1A)	1.363 (9)	B(15)-OH(7)	1.470 (10)
B(1)-O(2A)	1.365 (10)	B(15)-O(4A)	1.478 (11)
B(2)-O(4)	1.371 (11)	B(15)-OH(6A)	1.480 (10)
B(2)-O(5)	1.359 (11)	B(16)-O(7)	1.463 (10)
B(2)-O(6)	1.367 (13)	B(16)-O(11)	1.458 (12)
B(3)-O(7)	1.333 (9)	B(16)-O(26)	1.476 (10)
B(3)-OH(1)	1.393 (10)	B(16)-OH(8)	1.467 (13)
B(3)-O(9A)	1.361 (9)	B(17)-O(1)	1.464 (10)
B(4)-O(10)	1.355 (9)	B(17)-O(6)	1.475 (11)
B(4)-O(12)	1.363 (10)	B(17)-O(14)	1.448 (9)
B(4)-OH(2)	1.385 (10)	B(17)-OH(9)	1.464 (12)
B(5)-O(14)	1.362 (10)	B(18)-O(24)	1.478 (10)
B(5)-OH(4)	1.390 (11)	B(18)-O(25)	1.481 (11)
B(5)-O(13A)	1.339 (10)	B(18)-OH(10)	1.473 (13)
		B(18)-OH(11)	1.469 (10)
		B(19)-O(5)	1.494 (10)
B(6)-O(16)	1.379 (10)	B(19)-OH(12)	1.477 (11)
B(6)-O(17)	1.373 (9)	B(19)-O(28B)	1.481 (12)
B(6)-O(18)	1.372 (9)	B(19)-OH(16)	1.456 (10)
B(7)-O(20)	1.372 (9)	B(20)-O(20)	1.471 (12)
B(7)-O(21)	1.347 (10)	B(20)-O(34)	1.488 (10)
B(7)-O(19A)	1.389 (11)	B(20)-OH(14)	1.477 (10)
B(8)-O(22)	1.387 (9)	B(20)-OH(15)	1.467 (11)
B(8)-O(24)	1.357 (10)		
B(8)-O(23A)	1.361 (10)	B(21)-O(13)	1.512 (10)
		B(21)-O(32)	1.472 (9)
		B(21)-OH(16)	1.448 (12)
B(9)-O(25)	1.376 (10)	B(21)-O(33B)	1.495 (10)
B(9)-O(26)	1.357 (9)		
B(9)-O(27)	1.361 (10)	B(22)-O(15)	1.484 (11)
		B(22)-O(18)	1.464 (9)
B(10)-O(28)	1.355 (10)	B(22)-O(19)	1.455 (11)
B(10)-O(30)	1.383 (11)	B(22)-O(10A)	1.477 (9)
B(10)-O(29A)	1.357 (12)		
		B(23)-O(8)	1.470 (14)
B(11)-OH(5)	1.380 (11)	B(23)-O(30)	1.469 (12)
B(11)-O(31A)	1.358 (10)	B(23)-OH(18)	1.483 (12)
B(11)-O(33A)	1.363 (12)	B(23)-OH(1M)	1.465 (12)
B(12)-O(8)	1.360 (10)	B(24)-O(17)	1.488 (10)
B(12)-O(11)	1.380 (12)	B(24)-O(27)	1.463 (9)
B(12)-O(34)	1.355 (11)	B(24)-OH(19)	1.478 (12)
B(13)-O(9)	1.461 (11)	B(24)-OH(20)	1.457 (10)
B(13)-O(15)	1.452 (10)		
B(13)-OH(3)	1.466 (12)	B(25)-O(3)	1.475 (10)
B(13)-O(12B)	1.497 (11)	B(25)-OH(21)	1.499 (10)
B(14)-O(22)	1.460 (10)	B(25)-OH(22)	1.469 (12)
B(14)-O(29)	1.488 (12)		
B(14)-O(32)	1.429 (12)	B(26)-O(2)	1.464 (9)
B(14)-O(31B)	1.502 (10)	B(26)-O(23)	1.498 (10)
		B(26)-OH(23)	1.457 (12)
		B(26)-OH(2F)	1.476 (10)

structure refined only to an *R* index of 9.3%. Because of the high correlations of atomic parameters between the subcell and the true cell, the boron – oxygen bond distances were constrained. This did not result in a lower value of the *R* index, but gave more reliable positions of the oxygen atoms, and hence lower standard deviations in the bond lengths. The final positional parameters and isotropic displacement factors are given in Table 4, and selected interatomic distances, in Table 5; observed and calculated structure-factors may be obtained from the Depository of Unpublished Data, CISTI, National Research Council of Canada, Ottawa, Ontario, Canada K1A 0S2.

TABLE 4. RUITENBERGITE: ATOMIC COORDINATES ( $\text{\AA} \times 10^4$ )  
AND ISOTROPIC DISPLACEMENT FACTORS ( $\text{\AA}^2 \times 10^2$ )

	<i>x</i>	<i>y</i>	<i>z</i>	<i>U</i> (eq)
Ca1	907(9)	3479	173(11)	12(4)
Ca2	918(11)	5478(18)	3208(11)	15(4)
Ca3	4139(11)	5599(22)	2336(12)	18(4)
Ca4	4083(10)	7729(18)	4281(11)	11(4)
Cals	891(10)	3394(15)	5129(11)	14(4)
Ca2s	962(10)	5451(17)	8271(11)	13(4)
Ca3s	4125(10)	5695(21)	7345(11)	14(4)
Ca4s	4064(11)	7617(10)	9296(11)	16(4)
Ca5s	2142(6)	9425(15)	9715(7)	19(4)
B1	5425(33)	10055(54)	4378(29)	12
B2	567(30)	6242(56)	1122(18)	10
B3	2518(24)	5985(74)	2760(28)	15
B4	5499(31)	3440(63)	3603(29)	10
B5	397(27)	2741(55)	1856(26)	10
B6	2598(27)	4968(46)	234(25)	10
B7	-87(29)	7641(50)	1877(21)	10
B8	1406(14)	4438(26)	1987(14)	10
B9	3518(16)	6794(29)	508(18)	10
B10	5035(24)	5020(36)	4588(34)	11
B11	5209(29)	3652(50)	2143(15)	15
B12	2515(12)	6832(26)	4101(15)	0
B13	-115(54)	11358(98)	389(56)	24
B1s	5360(31)	9902(72)	9248(34)	10
B2s	519(29)	6352(45)	6135(14)	11
B3s	2499(21)	5817(74)	7801(21)	10
B4s	5629(29)	3627(69)	8624(23)	10
B5s	465(27)	2526(52)	6812(21)	9
B6s	2538(26)	4902(50)	5072(18)	17
B7s	20(28)	7672(43)	7050(29)	10
B8s	1398(14)	4431(25)	6858(14)	11
B9s	3561(18)	6523(26)	5579(16)	5
B10s	5029(22)	5047(40)	9464(35)	10
B11s	5010(30)	3459(33)	6986(16)	10
B12s	2506(14)	6678(24)	9136(16)	12
B13s	-98(44)	11156(79)	5502(45)	10
O1	3198(25)	5673(46)	787(22)	29(15)
O2	5053(20)	9375(41)	4751(23)	0(9)
O3	1061(18)	5200(31)	1185(17)	0(8)
O4	64(21)	7282(40)	2731(16)	7(8)
O5	5225(33)	4252(42)	2928(16)	41(15)
O6	3096(24)	7394(37)	4868(20)	26(16)
O7	1869(19)	5368(48)	2677(25)	27(13)
O8	4057(16)	6058(34)	304(22)	0(7)
O9	897(16)	3699(32)	2270(18)	0(7)

#### DESCRIPTION OF THE STRUCTURES

##### Pringleite

The triclinic polymorph, pringleite, has a three-dimensional framework consisting of 26 crystallographically distinct borate polyhedra, 12 of which are triangular  $[(\text{BO}_3)]$  groups and 14 of which are tetrahedral  $[(\text{BO}_4)]$  groups (Figs. 1a, b). Those anions bonded to two B atoms are  $\text{O}^{2-}$  (oxygen) atoms, anions bonded to one B atom are  $(\text{OH})^-$  (hydroxyl) groups, and oxygen atoms not bonded directly to B atoms form  $(\text{H}_2\text{O})^0$  groups. The assignment of  $\text{O}^{2-}$ ,  $(\text{OH})^-$  and  $(\text{H}_2\text{O})^0$  was checked by bond-valence calculations. Figures 1a and 1b show  $(\text{BO}_n)$  polyhedra, whereas in all subsequent figures, B-B connectivity diagrams are used, as eliminating the anions greatly simplifies the illustration; in these figures, B atoms connected by a line are those sharing an anion (cf. Fig. 1c).

TABLE 4 — (Cont'd.)

010	3979(20)	7344(41)	1335(17)	0(9)
011	4528(20)	8910(38)	664(23)	0(7)
012	2226(30)	5559(49)	4296(24)	80(20)
013	473(22)	2337(40)	1149(19)	3(8)
014	396(27)	6599(48)	1775(23)	30(15)
015	143(22)	6842(42)	361(18)	0(9)
016	4723(21)	4408(46)	1373(21)	15(10)
017	2883(15)	6625(35)	3532(15)	0(7)
OH1	1837(44)	3587(81)	1666(54)	96(24)
OH2	689(22)	2797(44)	3751(24)	7(8)
OH3	-409(38)	4945(72)	4248(43)	64(19)
OH4	4391(18)	5269(49)	3804(21)	16(11)
OH5	808(19)	5795(41)	4518(22)	0(7)
OH6	4128(21)	8277(42)	2984(23)	0(8)
OH7	1831(26)	7627(80)	3754(47)	71(21)
OH8	5535(19)	6380(26)	4587(22)	0(7)
OH9	2835(19)	5674(42)	2197(20)	0(7)
OH10	5316(23)	7078(41)	3071(25)	6(9)
OH11	2270(44)	3774(54)	344(55)	80(22)
OH12	-231(38)	4065(76)	2975(41)	73(19)
01s	3117(16)	5435(33)	5748(16)	0(7)
02s	4931(23)	9518(52)	9644(26)	22(12)
03s	865(21)	5191(31)	6117(19)	13(11)
04s	-155(19)	6988(34)	7704(18)	0(7)
05s	5214(20)	4070(33)	7818(12)	0(8)
06s	2981(20)	7519(34)	9857(17)	0(8)
07s	1828(15)	5251(38)	7582(19)	0(9)
08s	5859(24)	11058(37)	4820(27)	35(11)
09s	1001(27)	3506(48)	7179(26)	47(16)
010s	3898(28)	7569(45)	6245(26)	24(14)
011s	4354(42)	9077(77)	5620(47)	67(20)
012s	2337(19)	5351(27)	9393(21)	0(6)
013s	290(20)	2198(37)	5993(15)	0(8)
014s	495(19)	6743(38)	6845(17)	0(9)
015s	69(37)	6754(78)	5362(23)	51(19)
016s	4687(19)	4713(30)	6515(20)	0(7)
017s	2862(22)	6267(77)	8586(22)	85(21)
OH1s	1860(17)	3446(34)	6658(22)	0(7)
OH2s	831(22)	3026(43)	8701(25)	4(9)
OH3s	-206(19)	4827(37)	9504(21)	0(7)
OH4s	4260(16)	5137(43)	8787(19)	0(9)
OH5s	823(22)	6231(46)	9520(26)	10(9)
OH6s	4009(41)	8383(78)	7884(45)	57(20)
OH7s	1815(16)	7462(38)	8707(23)	0(8)
OH8s	5446(46)	6331(61)	9715(57)	100(26)
OH9s	2928(18)	5955(40)	7370(22)	3(8)
OH10s	5170(21)	7317(40)	8073(23)	0(8)
OHs11	-2213(19)	3867(32)	5313(24)	0(7)
OHs12	-292(20)	4168(39)	7818(23)	0(7)
C11	1740(13)	636(28)	3573(14)	50(337)
C12	1898(10)	9585(26)	2107(11)	42(7)
C13s	3327(8)	2716(22)	8780(11)	32(6)
C14s	2893(9)	715(22)	7218(11)	34(6)
W2	3496(25)	3358(51)	1929(28)	21(10)
W3	1432(20)	1029(37)	326(22)	2(7)
W5	3341(34)	9819(64)	4044(37)	45(15)
W7	2038(21)	7854(39)	724(24)	9(8)
W10	3032(37)	3108(71)	3685(40)	53(17)
W1s	1855(29)	1212(59)	8709(34)	33(13)
W2s	3651(36)	3105(67)	7235(39)	51(17)
W3s	1670(28)	1211(53)	5487(32)	22(12)
W5s	3329(31)	9692(60)	-1264(33)	38(13)
W6s	3144(20)	706(43)	5607(23)	12(8)
W7s	1853(32)	7788(64)	5462(37)	41(15)
W8s	809(22)	9397(49)	9001(25)	25(9)
W9s	1684(27)	8515(54)	7069(30)	30(11)

Polymerization of the borate polyhedra is strongest within the (110) plane (Fig. 1c), which is the plane normal to the acute bisectrix of the biaxial indicatrix. This plane is composed of 12-membered borate rings of average composition  $[\text{B}_{12}\text{O}_{21}(\text{OH})_9]^{13-}$  that are linked to form a sheet. The 12-membered ring consists of six alternating triangular and six tetrahedral poly-

TABLE 5. RUITENBERGITE: INTERATOMIC DISTANCES (Å)

Ca1-O3	2.361(33)	Cals-OH2	2.349(47)
Ca1-O13	2.476(47)	Cals-OH3	2.826(67)
Ca1-OH1	2.497(75)	Cals-OH5	2.541(42)
Ca1-OH11	2.611(94)	Cals-O3s	2.475(39)
Ca1-W3	2.566(37)	Cals-O13s	2.564(45)
Ca1-O15A	2.473(42)	Cals-OH1s	2.565(33)
Ca1-OH2B	2.559(51)	Cals-OHs1	2.550(45)
Ca1-OH3B	2.411(37)	Cals-W3s	2.544(53)
Ca1-OH5B	2.884(45)	Cals-O15C	2.353(72)
Ca2-O4	2.336(42)	Ca2s-O4s	2.508(38)
Ca2-O7	2.433(53)	Ca2s-O7s	2.487(44)
Ca2-O9	2.373(38)	Ca2s-O9s	2.712(53)
Ca2-O12	2.500(48)	Ca2s-O12s	2.617(34)
Ca2-O14	2.529(43)	Ca2s-O14s	2.595(35)
Ca2-OH2	2.871(48)	Ca2s-OH2s	2.518(47)
Ca2-OH5	2.415(47)	Ca2s-OH5s	2.439(54)
Ca2-OH7	2.666(68)	Ca2s-OH7s	2.486(38)
Ca2-OH12	2.544(79)	Ca2s-OHs2	2.594(43)
Ca3-O1	2.575(36)	Ca3s-O1s	2.687(28)
Ca3-O5	2.359(57)	Ca3s-O5s	2.521(40)
Ca3-O10	2.362(41)	Ca3s-O10s	2.550(49)
Ca3-O16	2.675(52)	Ca3s-O16s	2.370(47)
Ca3-OH4	2.428(43)	Ca3s-OH4s	2.487(40)
Ca3-OH6	2.841(47)	Ca3s-OH6s	2.817(81)
Ca3-OH9	2.499(44)	Ca3s-OH9s	2.409(44)
Ca3-OH10	2.582(43)	Ca3s-OHs0	2.490(40)
Ca3-W2	2.472(53)	Ca3s-W2s	2.664(69)
Ca4-O2	2.371(42)	Ca4s-O2s	2.422(51)
Ca4-O6	2.586(55)	Ca4s-O6s	2.714(49)
Ca4-O17	2.436(32)	Ca4s-O17s	2.546(54)
Ca4-OH4	2.684(50)	Ca4s-OH4s	2.652(46)
Ca4-OH6	2.371(49)	Ca4s-OH6s	2.541(86)
Ca4-OH8	2.690(40)	Ca4s-OH8s	2.819(87)
Ca4-O11s	2.541(82)	Ca4s-O8A	2.330(43)
Ca4-W5	2.438(66)	Ca4s-O11A	2.515(41)
Ca4-O8sA	2.232(47)	Ca4s-W5s	2.440(59)
		Ca5s-O6s	2.431(39)
		Ca5s-OH7s	2.493(40)
		Ca5s-W8s	2.410(41)
		Ca5s-W3A	2.613(46)
		Ca5s-W7A	2.408(46)
		Ca5s-W1sA	2.366(59)
B1-02	1.345(80)	B1s-O2s	1.356(90)
B1-O8s	1.317(62)	B1s-O8B	1.567(69)

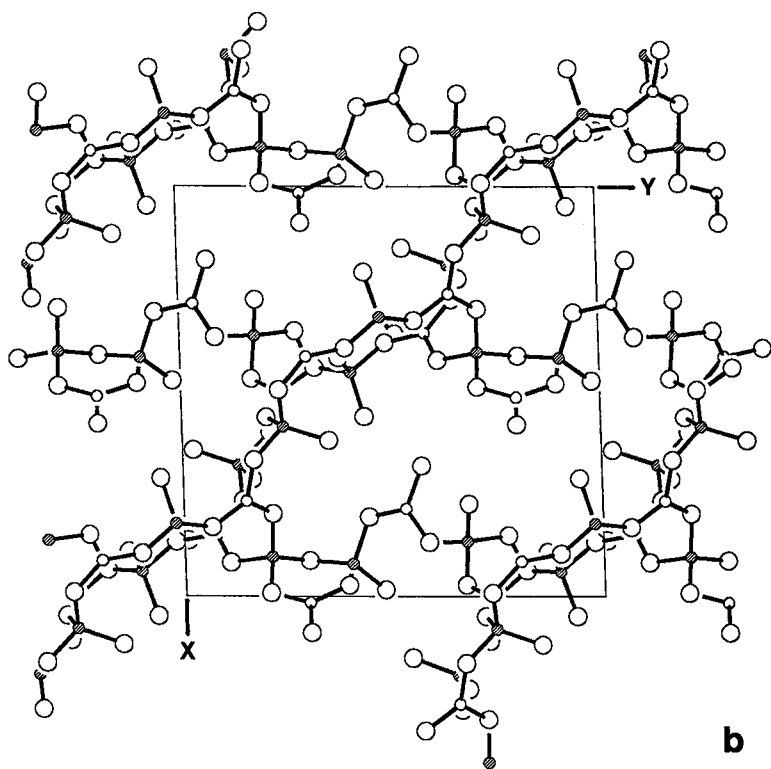
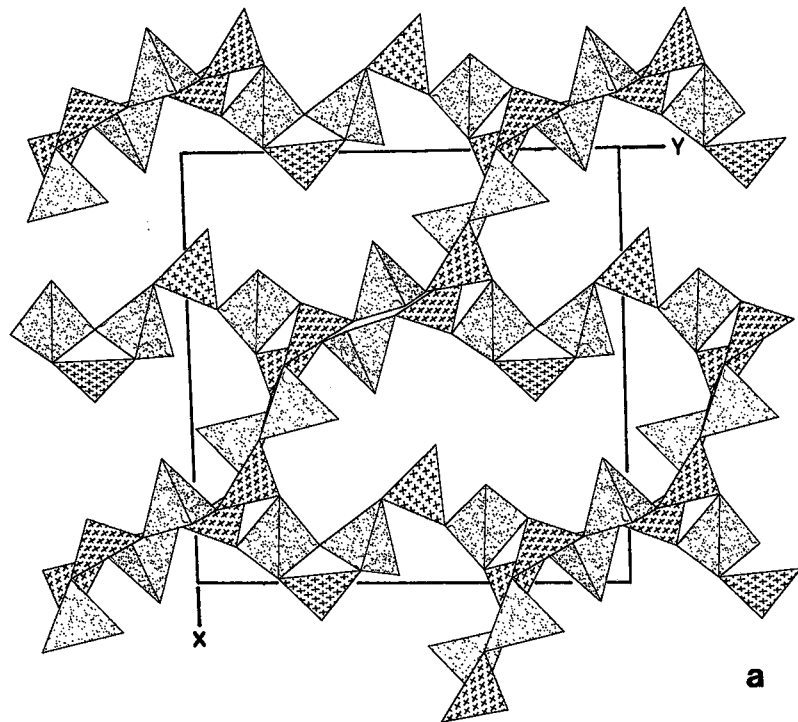
hedra (Fig. 2). These planes of 12-membered borate rings are cross-linked or hooked to each other by other borate polyhedra, as seen in Figure 1c (circled). One end of the hook is a triangular borate group attached to a borate tetrahedron within one (110) plane, whereas the other end of the hook consists of a triangular and a tetrahedral borate group attached to a tetrahedral borate group in the adjacent (110) plane. The significance of this "hooked", tetrahedral – tetrahedral – triangular, 3-membered ring will become more evident in a comparison of the polymorphic structures.

The borate polymerization in pringleite is zeolite-like, with large channels (with a free aperture of approximately  $10 \times 3$  Å) parallel to the Z axis, and a smaller channel (with a free aperture of approximately  $6 \times 2$  Å) parallel to [110]. The channels parallel to the Z axis are bounded by 18-membered rings, and provide space for the Ca and Cl atoms as well as the H<sub>2</sub>O groups. These interstitial constituents also are present in layers parallel to the (110) plane (Fig. 3). Ca atoms (Ca1 to Ca8) are [9]-coordinated in layers that sand-

TABLE 5 — (Cont'd.)

B1-016B	1.521(64)	B1s-016A	1.138(74)
B2-03	1.382(66)	B2s-03s	1.326(60)
B2-014	1.366(71)	B2s-014s	1.321(51)
B2-015	1.375(45)	B2s-015s	1.333(49)
B3-07	1.372(68)	B3s-07s	1.340(55)
B3-017	1.387(56)	B3s-017s	1.332(56)
B3-0H9	1.407(71)	B3s-0H9s	1.361(64)
B4-05	1.333(61)	B4s-05s	1.373(44)
B4-010B	1.397(80)	B4s-010A	1.454(76)
B4-011C	1.410(97)	B4s-011B	1.433(69)
B5-09	1.333(56)	B5s-09s	1.370(66)
B5-013	1.365(66)	B5s-013s	1.365(47)
B5-04sA	1.292(68)	B5s-04A	1.583(70)
B6-01	1.365(56)	B6s-012	1.391(52)
B6-0H11	1.383(86)	B6s-01s	1.363(43)
B6-012A	1.393(54)	B6s-0Hs1	1.352(64)
B7-04	1.441(48)	B7s-04s	1.486(68)
B7-014	1.455(76)	B7s-014s	1.454(69)
B7-0H2C	1.448(56)	B7s-0H2A	1.523(51)
B7-0HsB	1.648(61)	B7s-0H1B	1.421(87)
B8-03	1.479(36)	B8s-03s	1.484(35)
B8-07	1.482(44)	B8s-07s	1.438(37)
B8-09	1.482(47)	B8s-09s	1.454(62)
B8-0H1	1.461(104)	B8s-0H1s	1.466(47)
B9-01	1.443(58)	B9s-06	1.469(40)
B9-08	1.451(51)	B9s-01s	1.483(47)
B9-010	1.455(38)	B9s-01s0	1.480(48)
B9-06sA	1.385(38)	B9s-08sA	1.639(66)
B10-0H4	1.454(50)	B10s-0H4s	1.495(45)
B10-0H8	1.464(48)	B10s-0H8s	1.459(74)
B10-02A	1.391(74)	B10s-01B	1.486(63)
B10-011C	1.678(104)	B10s-02sA	1.615(78)
B11-05	1.482(55)	B11s-05s	1.466(38)
B11-016	1.484(47)	B11s-016s	1.463(42)
B11-0H6B	1.596(106)	B11s-0h6A	1.700(75)
B11-0hsA	1.466(62)	B11s-0h1A	1.473(55)
B12-06	1.463(37)	B12s-06s	1.469(35)
B12-012	1.463(59)	B12s-012s	1.450(40)
B12-017	1.473(44)	B12s-017s	1.468(61)
B12-0h7	1.456(60)	B12s-0h7s	1.472(38)
B13-013A	1.656(93)	B13s-0h3A	1.490(105)
B13-015B	1.375(113)	B13s-0h5A	1.439(100)
B13-0h3C	1.597(104)	B13s-013B	1.343(80)
B13-0h5C	1.485(129)	B13s-015D	1.644(104)
C11-0H2	3.03(9)	C13-0H4s	2.97(12)
C11-0H7	3.15(9)	C13-0H8s	3.22(10)
C11-0Hs2	3.13(8)	C13-W1s	3.26(11)
C11-W5	3.08(8)	C13-W2s	3.14(12)
C11-W3s	3.46(7)	C13-W5s	2.90(9)
C11-W6s	3.48(11)		
C12-0H3s	3.37(9)		
C12-0Hs2	3.20(10)		
C12-W3	3.18(8)		
C12-W5	3.39(9)		
C12-W7	3.02(8)		
		C14-0H1s	3.22(10)
		C14-0H6s	3.04(11)
		C14-W2s	2.71(12)
		C14-W5s	2.59(13)
		C14-W9s	3.11(11)

which the borate layers. The H<sub>2</sub>O groups and Cl atoms form a broad slab between the layers of (CaO<sub>n</sub>) polyhedra. The Cl atoms are not bonded to Ca, but are hydrogen-bonded to OH and H<sub>2</sub>O groups. This coordination of Cl occurs in several synthetic compounds and two borate minerals, hydrochlorborite (Brown & Clark 1978) and wiserite (Pertlik & Dunn 1989). In



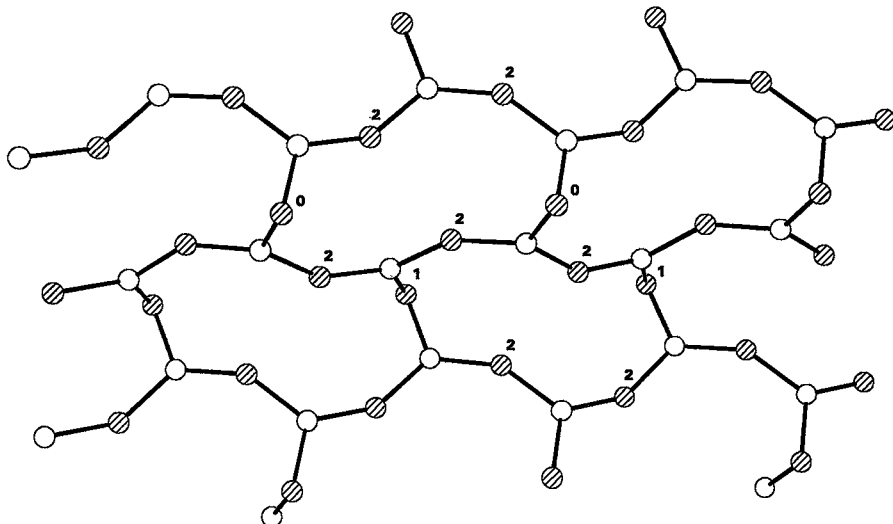
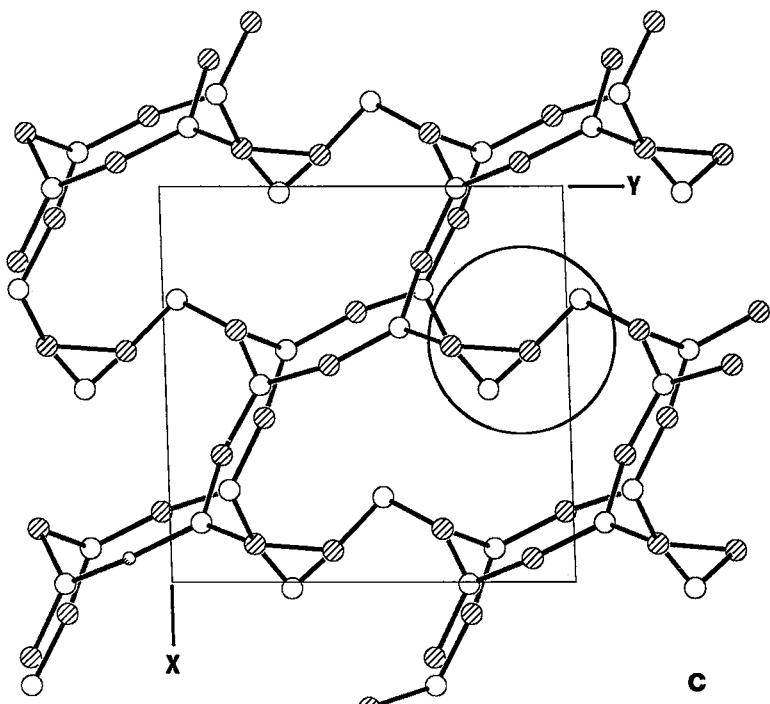


FIG. 2. Pringleite, (110) plane showing B–B connectivity. The 12-membered rings have alternating B polyhedra in triangular coordination (open circles) and tetrahedral coordination (lined circles). The small numbers differentiate the tetrahedra with respect to numbers of OH ligands.

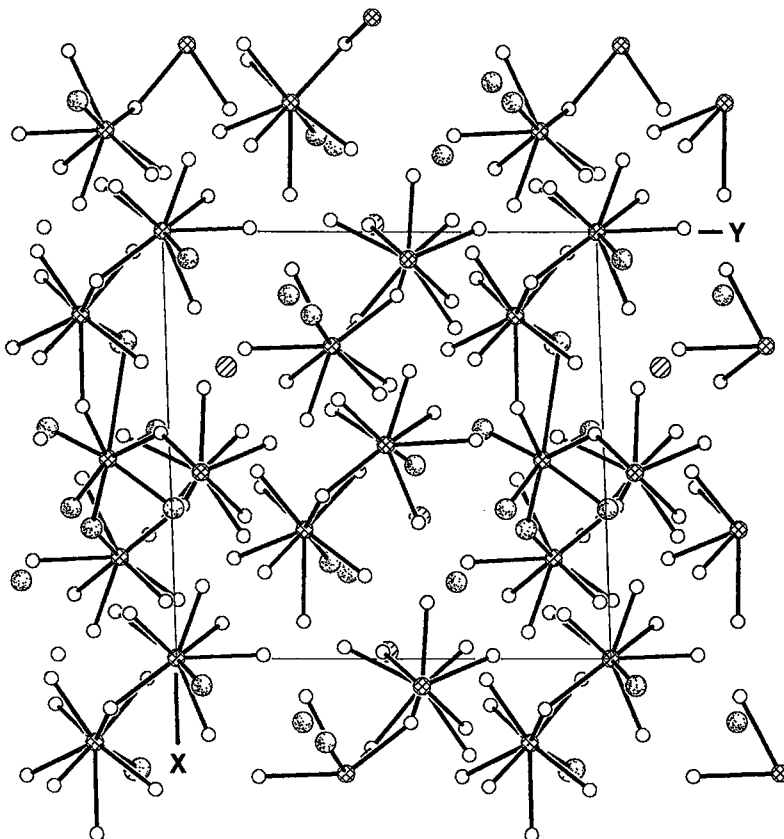


FIG. 3. Pringleite, Z-axis projection showing (110) layering of Ca (cross-hatched) polyhedra, Cl atoms (lined) and  $\text{H}_2\text{O}$  molecules (dot shaded).

pringleite, the  $\text{OH} \dots \text{Cl}$  hydrogen-bond distances are typically in the range 3.1 to 3.4 Å (Table 3); Cl1 and Cl3 have five, and Cl2 and Cl4 have seven incident hydrogen bonds. These hydrogen bonds fix the Cl within the structure, as is apparent from the standard deviations, which are comparable in size to those of the Ca atoms. The  $\text{H}_2\text{O}$  groups W1 to W10 are bonded to Ca atoms, whereas W11 to W13 are only hydrogen-bonded within the structure. The Ca9 atom is distinct from other Ca atoms in that it is not in the Ca layer but in the  $\text{H}_2\text{O}-\text{Cl}$  layer, and is [7]-coordinated.

#### Ruitenbergite

The monoclinic polymorph, ruitenbergite, has a structure similar to that of pringleite, but with sufficient rearrangement of the structural units to distinguish the dimorphs by X-ray powder diffraction (Roberts *et al.* 1993). Like pringleite, ruitenbergite has a three-dimensional borate framework consisting of 26 symmetrically unique boron–oxygen polyhedra. As in pringleite, 12 of these polyhedra contain boron in

triangular coordination, and the other 14 have boron in tetrahedral coordination. It is the way in which these two types of polyhedra polymerize that distinguishes the two minerals.

As in pringleite, the plane of 12-membered borate rings defines the layering of Ca,  $\text{H}_2\text{O}$  groups and Cl (Fig. 4). Six of the Ca atoms are [9]-coordinated, two are [8]-coordinated, and the unique  $\text{Ca5s}$  atom is [6]-coordinated. The four Cl atoms are hydrogen-bonded to OH and  $\text{H}_2\text{O}$  groups, with the following coordinations: Cl1 with  $3 \times \text{OH}$  and  $3 \times \text{H}_2\text{O}$ ; Cl2 with  $3 \times \text{OH}$  and  $3 \times \text{H}_2\text{O}$ ; Cl3 with  $3 \times \text{OH}$  and  $3 \times \text{H}_2\text{O}$ ; Cl4 with  $2 \times \text{OH}$  and  $2 \times \text{H}_2\text{O}$  in the 3.0 to 3.6 Å range. Nine of the  $\text{H}_2\text{O}$  groups are bonded directly to Ca atoms, whereas four other  $\text{H}_2\text{O}$  groups (W10, W6s, W7s, W9s) are solely involved in hydrogen-bonding. The supercell in ruitenbergite (which doubles the *c* cell parameter) is a result of variations of Cl and  $\text{H}_2\text{O}$  sites in the two halves of the cell. This rearrangement, as well as the consistency in the two halves with respect to Ca sites and the borate framework, are best seen in Figure 5.

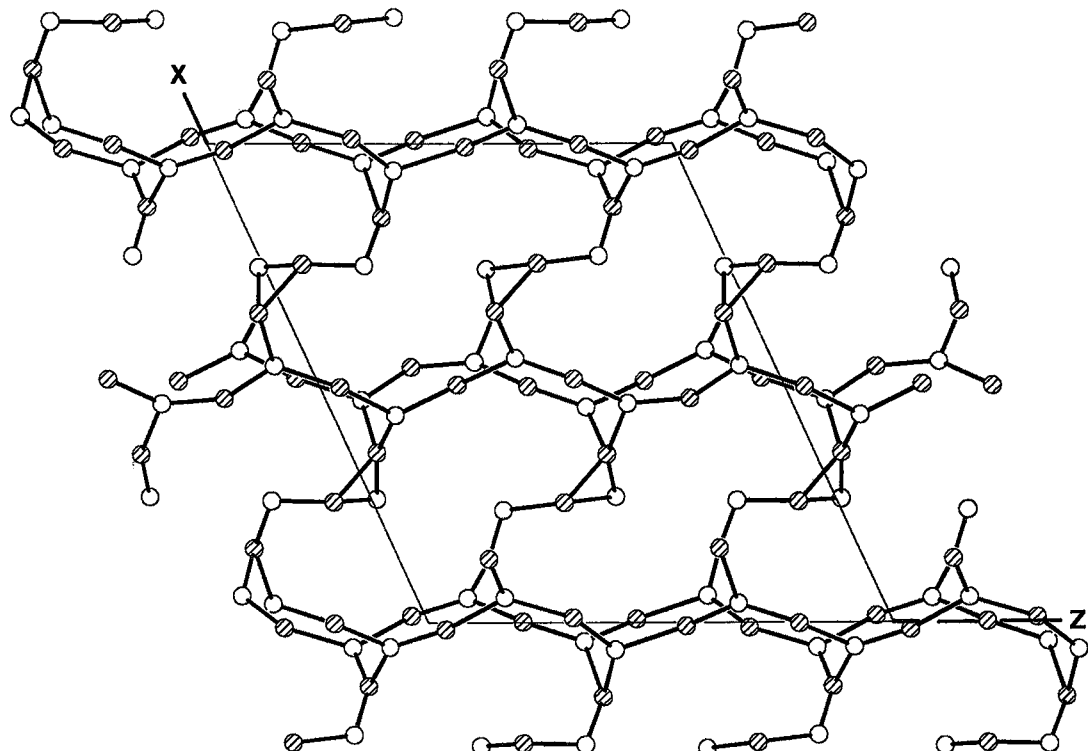


FIG. 4. Ruitenbergite, Y-axis projection of B-B connectivity framework. Boron coordination polyhedra are differentiated by open circles (triangular) and lined circles (tetrahedral).

#### COMPARISON OF THE TWO STRUCTURAL FRAMEWORKS

The relationship between the orientations of the two structures is shown in Figure 5. The orientation matrix to transform from the triclinic structure of pringleite to the monoclinic structure of ruitenbergite is  $101/10\bar{1}/0\bar{1}0$ . Figure 4 shows the strong polymerization of borate polyhedra in the (100) plane in ruitenbergite, which is comparable to the (110) plane in pringleite (Fig. 2). Figures 6a and 6b show the connected 12-membered rings. The polymerization of the borate polyhedra differ in a subtle but significant fashion. In pringleite and ruitenbergite, the layers of 12-membered rings consist of alternating triangular ( $\Delta$ ) and tetrahedral ( $T$ ) polyhedra. Both have a fundamental building-block (FBB) [12:6 $\Delta$ +6 $T$ ] (nomenclature of Christ & Clarke 1977).

The classification scheme of Christ & Clarke (1977) does not differentiate between the different types of triangular and tetrahedral coordination possible for B. In pringleite and ruitenbergite, there are two types of triangles,  $\text{BO}_3$  and  $\text{BO}_2\text{OH}$ , and three

types of tetrahedra,  $\text{BO}_4$ ,  $\text{BO}_3\text{OH}$  and  $\text{BO}_2(\text{OH})_2$ . If we modify the classification scheme of Christ & Clark (1977) to indicate the number of H atoms in each polyhedron (through the use of superscripts), we get  $\Delta^0$ ,  $\Delta^1$ ,  $T^0$ ,  $T^1$  and  $T^2$  for each possibility listed above. Thus the (110) layer in pringleite consists of alternating rings of  $[12:6\Delta^0+4T^2+2T^0]$ , and  $[12:6\Delta^0+4T^2+2T^1]$ , arranged as shown in Figure 2. For ruitenbergite, the (100) layer at  $x \approx 0$  (Fig. 6a) contains  $[12:6\Delta^0+4T^2+2T^1]$  with a composition  $[\text{B}_{12}\text{O}_{20}(\text{OH})_{10}]^{14-}$ , and the (100) layer at  $x \approx 1/2$  (Fig. 6b) contains  $[12:6\Delta^0+4T^2+2T^1]$ , with a composition  $[\text{B}_{12}\text{O}_{22}(\text{OH})_8]^{12-}$ . These different arrangements of polyhedra in the layers of 12-membered rings in turn affect the intraplanar linkage. Figure 7 compares the layering in pringleite and ruitenbergite. The  $L_2$  layers in each structure, consisting of sheets of 12-membered rings, are identical in topology but differ in the way they connect to subsequent cross-linkage layers,  $L_1$ . In pringleite,  $L_1$  and  $L_2$  layers alternate regularly, whereas in ruitenbergite, the sequence is  $L_1 L_2 L_1' L_2 L_1 \dots$ , where  $L_1'$  is related to  $L_1$  by a  $2_1$  symmetry operator. Figure 7 shows that the

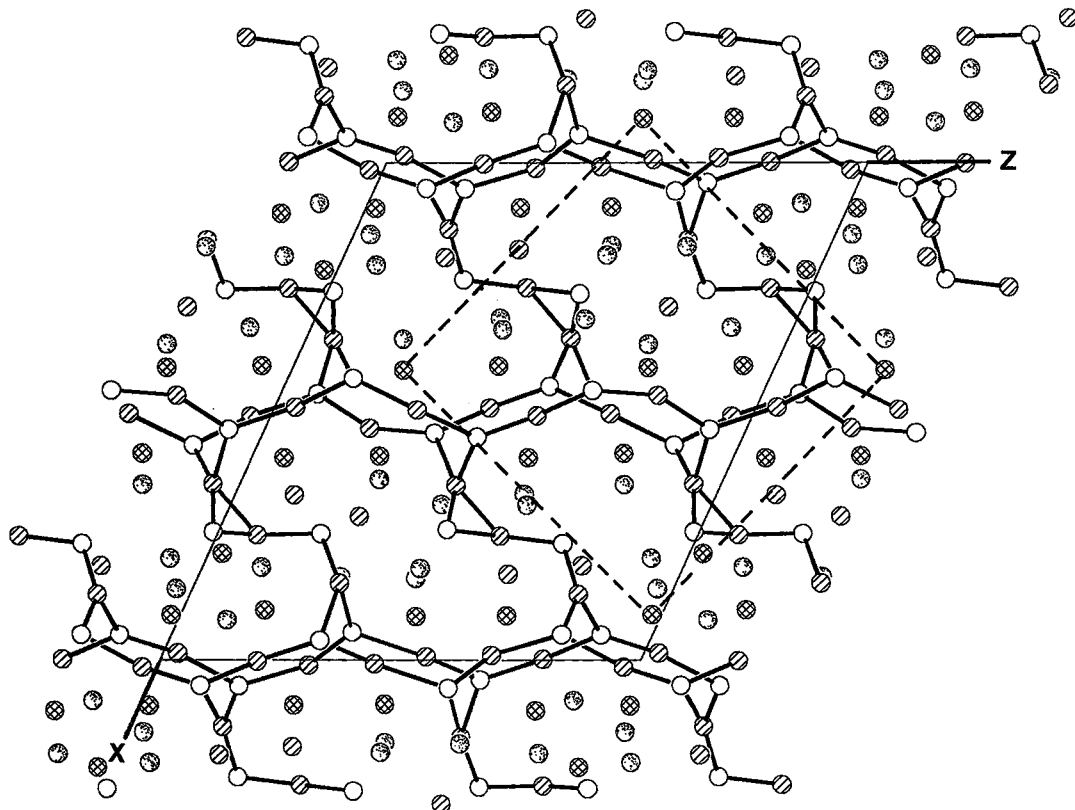


FIG. 5. Ruitenbergite, Y-axis projection of B-B connectivity with Ca atoms (cross-hatched), Cl atoms (lined), and \$H\_2O\$ molecules (shaded). The corresponding Z-axis projection of pringleite has a dashed outline.

\$T^0\$ tetrahedron is the only B polyhedron to be connected to four other B polyhedra. This gives it the distinction of attaching the 3-membered ring of the cross-linkage layer, \$L1\$, whereas the simple termination of the cross-linkage, \$\Delta^1\$, links to a \$T^1\$ in the ring of an adjacent layer. The two distinct 12-membered rings in ruitenbergite *versus* the single mixed-layer of 12-membered rings in pringleite introduces a \$2\_1\$ axis in the former structure.

#### COMPARISON WITH OTHER BORATE STRUCTURES

The most complicated borate mineral FBB in the Christ & Clark (1977) classification scheme is [9:(4\$\Delta\$+5\$T\$)+2\$T\$], which is found in the crystal structure of preobrazhenskite (Rumanova *et al.* 1972). In pringleite and ruitenbergite, the borate ring plus the intralayer link has the FBB [12:(6\$\Delta\$+6\$T\$)+3:(2\$\Delta\$+17)]. Thus the fundamental building-blocks in both pringleite and ruitenbergite are considerably more complex than any previously described in other borate mineral structures.

The zeolitic borate polymorphs hilgardite-4M (Ghose & Wan 1979), hilgardite-3A (Wan & Ghose 1983) and hilgardite-1A (Rumanova *et al.* 1978) are chemically similar to pringleite and ruitenbergite, but structurally quite different. Each of these structures has distinct pentaborate polyanions linked to form a three-dimensional framework. Hilgardite-3A (Wan & Ghose 1983) has channels parallel to the Z axis; these channels consist of nine-membered borate rings with the FBB [9:(2\$\Delta\$+7\$T\$)], and the interstitial species occupy these channels.

Another mineral chemically similar to pringleite and ruitenbergite is hydrochlorborite: \$Ca\_2B\_4O\_4(OH)\_7Cl \cdot 7H\_2O\$. The borate-group polymerization in hydrochlorborite is considerably less complex than in the structures described here, with an FBB [3:(2\$T\$+\$\Delta\$)+\$T\$] that forms discrete units linked by Ca (Brown & Clark 1978). Solongoite, \$Ca\_2[B\_3O\_4(OH)\_4]Cl\$, has the same FBB as hydrochlorborite (Yamnova *et al.* 1974). There is no crystal-structure information on the only other (Ca,Cl) borate mineral, ekaternite, for comparison.

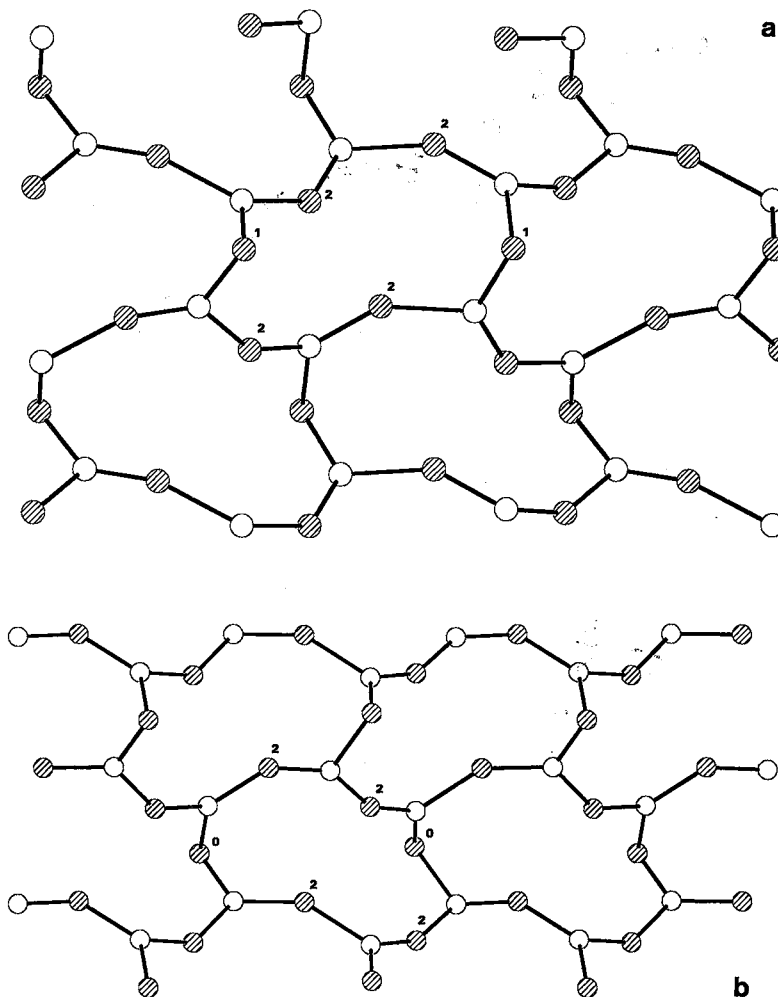


FIG. 6. Ruitenbergite (100) plane showing B-B connectivity at heights a)  $x = 0$ , b)  $x = \frac{1}{2}$ . In the 12-membered rings, B coordination polyhedra are differentiated by open circles (triangular) and lined circles (tetrahedral). The small numbers differentiate the tetrahedra with respect to the number of OH ligands.

#### *The role of Cl*

Although there are a large number of Ca borate minerals, it seems that the incorporation of Cl into this chemical class plays a unique and important crystalchemical role in the genesis of borate minerals. The Cl anion can have one or both of two contrasting structural roles: it may bond directly to the Ca atom, as in solongoite, it may H-bond to  $\text{H}_2\text{O}$  groups, as in hydrochlorborite, pringleite, and ruitenbergite, or it may adopt both roles, as in the hilgardite polymorphs.

The Cl-rich environment of this deposit resulted in

the crystallization of pringleite, ruitenbergite and hilgardite in association with halite and sylvite. Pringleite and ruitenbergite seem to have formed after hilgardite, perhaps in response to increased activities of B and  $\text{H}_2\text{O}$ . The relative increase in these components gives rise to the possibility of increased connectivity of B, as indicated by the change in structure from hilgardite to pringleite and ruitenbergite. In this saline environment, an even higher activity of  $\text{H}_2\text{O}$  might result in the formation of the less stable hydrochlorborite. It is also distinctly possible that this formation has been subjected to a relatively high grade of metamorphism, as evidenced by intense folding (Waugh & Urquhart

## PRINGLEITE

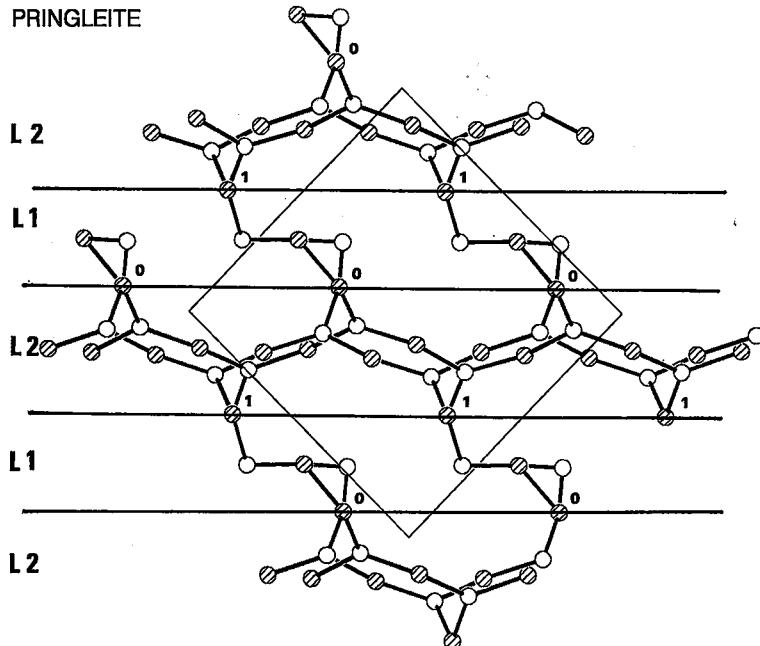
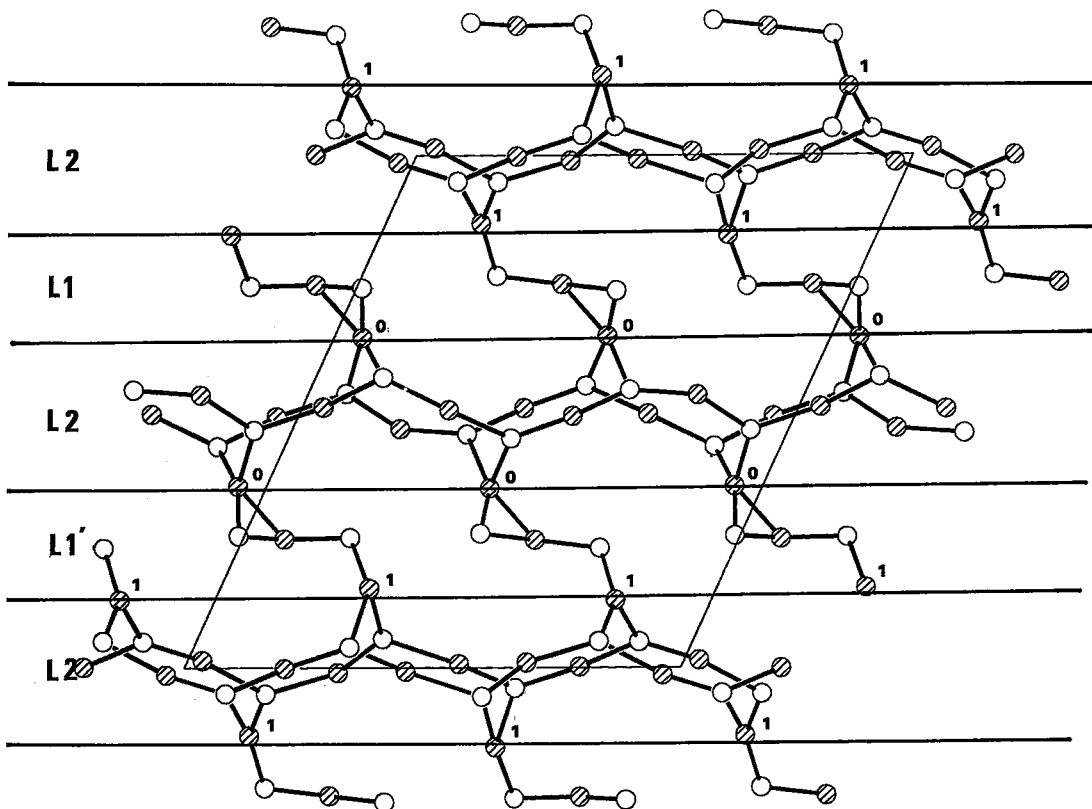


FIG. 7. Pringleite Z-axis projection and ruitenbergite Y-axis projection, juxtaposed to compare sequences of layers. B coordination polyhedra are differentiated by open circles (triangular) and lined circles (tetrahedral). Small numbers differentiate the tetrahedra with respect to numbers of OH ligands.

## RUITENBERGITE



1983). This could be an important factor in the crystallization of these newly discovered, unique minerals.

### SUMMARY

Pringleite and ruitenbergite are not only notable for their large, complex structures, but also serve as another example of natural phases that display new insight into structural chemistry. The tremendous increase in possibilities of polymerization in borates compared to silicates, due to the greater variety of coordination complexes, suggests new architectures that may be useful in zeolite-like compounds with applications in the materials sciences.

### ACKNOWLEDGEMENTS

The financial support of a Research Advisory Committee Grant from the Canadian Museum of Nature to JDG is gratefully acknowledged. The Natural Sciences and Engineering Research Council of Canada supported this work in the form of a Postgraduate Scholarship to PCB and Infrastructure, Major Equipment and Operating grants to FCH. The authors appreciate the improvements to this manuscript made possible by the suggestions of R.F. Martin, Emil Makovicky, R.T. Downs, and two anonymous referees.

### REFERENCES

- BROWN, G.E. & CLARK, J.R. (1978): Crystal structure of hydrochlorborite,  $\text{Ca}_2[\text{B}_3\text{O}_5(\text{OH})_4\cdot\text{OB}(\text{OH})_3]\text{Cl}\cdot7\text{H}_2\text{O}$ , a seasonal evaporite mineral. *Am. Mineral.* **63**, 814-823.
- BURNS, P.C., HAWTHORNE, F.C. & STIRLING, J.A.R. (1992): Trembachite,  $(\text{Mg},\text{Fe})_3\text{B}_7\text{O}_{13}\text{Cl}$ , a new borate mineral from the Salt Springs potash deposit, Sussex, New Brunswick. *Can. Mineral.* **30**, 445-448.
- CHRIST, C.L. & CLARK, J.R. (1977): A crystal-chemical classification of borate structures with emphasis on hydrated borates. *Phys. Chem. Minerals* **2**, 59-87.
- CROMER, D.T. & LIBERMAN, D. (1970): Relativistic calculation of anomalous scattering factors for X rays. *J. Chem. Phys.* **53**, 1891-1898.
- & MANN, J.B. (1968): X-ray scattering factors computed from numerical Hartree-Fock wave functions. *Acta Crystallogr.* **A24**, 321-324.
- GHOSE, S. & WAN, C. (1979): Hilgardite,  $\text{Ca}_2[\text{B}_5\text{O}_9]\text{Cl}\cdot\text{H}_2\text{O}$ : a piezoelectric zeolite-type pentaborate. *Am. Mineral.* **64**, 187-195.
- GRICE, J.D. & ERCIT, T.S. (1986): The crystal structure of moydite. *Can. Mineral.* **24**, 675-678.
- HAWTHORNE, F.C. & GRICE, J.D. (1990): Crystal-structure analysis as a chemical analytical method: application to first-row elements. *Can. Mineral.* **28**, 693-702.
- PERTLIK, F. & DUNN, P.J. (1989): Crystal structure of wiserite. *Am. Mineral.* **74**, 1351-1354.
- RACHLIN, A.L., MANDARINO, J.A., MUROWCHICK, B.L., RAMIK, R.A., DUNN, P.J. & BACK, M.E. (1986): Mineralogy of hilgardite-4M from evaporites in New Brunswick. *Can. Mineral.* **24**, 689-693.
- ROBERTS, A.C., STIRLING, J.A.R., GRICE, J.D., BURNS, P.C., ROULSTON, B.V., CURTIS, J.D. & JAMBOR, J.L. (1993): Pringleite and ruitenbergite, polymorphs of  $\text{Ca}_2\text{B}_{26}\text{O}_{34}(\text{OH})_{24}\text{Cl}_4\cdot13\text{H}_2\text{O}$ , two new mineral species from Sussex, New Brunswick. *Can. Mineral.* **31**, 795-800.
- ROULSTON, B.V. & WAUGH, D.C.E. (1981): A borate mineral assemblage from the Penobsquis and Salt Springs evaporite deposits of southern New Brunswick. *Can. Mineral.* **19**, 291-301.
- RUMANNOVA, I.M., IORYSH, Z.I. & BELOV, N.V. (1978): Crystal structure of triclinic chilgardite  $\text{Ca}_2[\text{B}_5\text{O}_9]\text{Cl}\cdot\text{H}_2\text{O}$  =  $\text{Ca}_2[\text{B}_3^{\pm}\text{B}_2^{\mp}\text{O}_9]\text{Cl}\cdot\text{H}_2\text{O}$ . *Sov. Phys. Dokl.* **22**, 460-462.
- , RAZMANOVA, Z.P. & BELOV, N.V. (1972): Crystal structure of preobrazhenskite  $3\text{MgO}\cdot5.5\text{B}_2\text{O}_3\cdot4.5\text{H}_2\text{O} = \text{Mg}_3[\text{B}_{11}\text{O}_{14}(\text{OH})_8\text{HO}_2]$ . *Sov. Phys. Dokl.* **16**, 518-521.
- SHELDICK, G.M. (1990): SHELLXTL, a crystallographic computing package, revision 4.1. Siemens Analytical Instruments, Inc., Madison, Wisconsin.
- WAN, C. & GHOSE, S. (1983): Parahilgardite,  $\text{Ca}_6[\text{B}_5\text{O}_9]_3\text{Cl}_3\cdot3\text{H}_2\text{O}$ : a triclinic piezoelectric zeolite-type pentaborate. *Am. Mineral.* **68**, 604-613.
- WAUGH, D.C.E. & URQUART, B.R. (1983): The geology of Denison - Potacan's New Brunswick potash deposit. *Sixth International Symposium on Salt* **1**, 85-98.
- YAMNOVA, N.A., EGOROV-TISMENKO, YU.K., SIMONOV, M.A. & BELOV, N.V. (1974): Crystal structure of solongoite  $\text{Ca}_2[\text{B}_3\text{O}_4(\text{OH})_4]\text{Cl}$ . *Sov. Phys. Dokl.* **19**, 326-327.

*Received March 3, 1993, revised manuscript accepted June 9, 1993.*